

# Reprogramming the Transition States to Enhance C–N Cleavage Efficiency of *Rhodococcus opacus* L-Amino Acid Oxidase

Published as part of JACS Au virtual special issue “Biocatalysis in Asia and Pacific”.

Yaoyun Wu, Yaozhong Cui, Wei Song, Wanqing Wei, Zhizhen He, Jinyang Tao, Dejing Yin, Xiulai Chen, Cong Gao, Jia Liu, Liming Liu, and Jing Wu\*



Cite This: JACS Au 2024, 4, 557–569



Read Online

ACCESS |

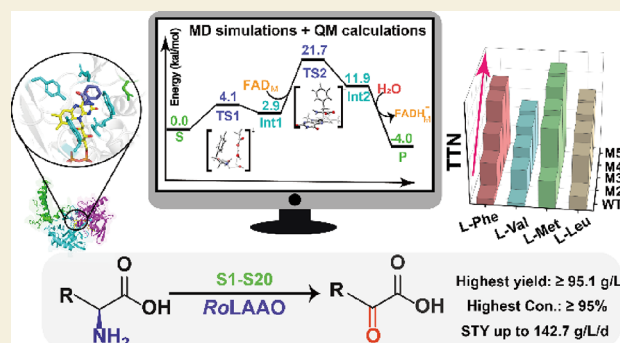
Metrics & More

Article Recommendations

Supporting Information

**ABSTRACT:** L-Amino acid oxidase (LAO) is an important biocatalyst used for synthesizing  $\alpha$ -keto acids. LAO from *Rhodococcus opacus* (RoLAO) has a broad substrate spectrum; however, its low total turnover number limits its industrial use. To overcome this, we aimed to employ crystal structure-guided density functional theory calculations and molecular dynamic simulations to investigate the catalytic mechanism. Two key steps were identified: S  $\rightarrow$  [TS1] in step 1 and Int1  $\rightarrow$  [TS2] in step 2. We reprogrammed the transition states [TS1] and [TS2] to reduce the identified energy barrier and obtain a RoLAO variant capable of catalyzing 19 kinds of L-amino acids to the corresponding high-value  $\alpha$ -keto acids with a high total turnover number, yield ( $\geq 95.1$  g/L), conversion rate ( $\geq 95\%$ ), and space-time yields  $\geq 142.7$  g/L/d in 12–24 h, in a 5 L reactor. Our results indicated the promising potential of the developed RoLAO variant for use in the industrial production of  $\alpha$ -keto acids while providing a potential catalytic-mechanism-guided protein design strategy to achieve the desired physical and catalytic properties of enzymes.

**KEYWORDS:** biocatalysts, reprogramming the transition states,  $\alpha$ -keto acids, protein engineering, C–N cleavage reaction



## INTRODUCTION

As green catalysts, enzymes are used in many industries,<sup>1,2</sup> such as the food,<sup>3</sup> pharmaceutical,<sup>4</sup> energy,<sup>5</sup> chemical,<sup>1</sup> and environmental protection industries,<sup>6</sup> as they can catalyze thousands of chemical reactions.<sup>2</sup> As biocatalysts, enzymes exhibit many advantages such as requiring mild reaction conditions,<sup>7</sup> low toxicity of reaction products,<sup>6,8</sup> low energy consumption,<sup>1</sup> and high specificity.<sup>9</sup> However, natural enzymes have some drawbacks that limit their industrial application. These drawbacks include low stability,<sup>6</sup> tolerability,<sup>10</sup> selectivity,<sup>11</sup> and catalytic efficiency.<sup>12</sup> These limitations are particularly important when using enzymes that can act on various substrates. However, such enzymes typically have low catalytic efficiency (total turnover number, TTN), resulting in low titer and conversion rates, which lower the efficiency of producing the desired chemicals.

To increase the catalytic efficiency of biocatalytic processes (i.e., to improve the TTN of enzymes), various protein engineering strategies have been developed, such as improving the catalytic stability of enzymes,<sup>6,13</sup> combining chemical enzymatic reactions,<sup>14,15</sup> cocompartmentalization of enzymes,<sup>16</sup> and mechanism-driven protein engineering. For example, the cocompartmentalization of aldo-keto reductase

(AKR) and cofactors in Pickering emulsion droplets for continuous flow catalysis significantly increased the TTN of AKR, by 4.22-fold compared with that of the control.<sup>16</sup> In contrast, with the rapid development of more advanced technologies for structural analysis, such as cryo-electron microscopy and intelligent computing methods including quantum mechanics/molecular mechanics (QM/MM),<sup>17–19</sup> the structures and catalytic mechanisms of action of specific enzymes have been deciphered.<sup>19–21</sup>

Determining the rate-limiting step of an enzyme based on structural mechanisms is critical for protein engineering. Experimental and computational methods have been used to determine the rate-limiting steps of enzymes. These methods are usually divided into detection techniques, isotopic tracing,<sup>22</sup> and crystallization experiments,<sup>21</sup> such as ultrahigh-performance liquid chromatography (UHPLC),<sup>6</sup> UV–vis

**Received:** October 30, 2023

**Revised:** December 21, 2023

**Accepted:** December 26, 2023

**Published:** January 16, 2024



Table 1. Performance Parameters of WT and the Variant M5 to Different L-Amino acids<sup>4a</sup>

S1-S20  $\xrightarrow[\text{Tris-HCl buffer (pH 8.0, 20 mM)}]{\text{L-amino acids oxidase}}$  P1-P20  
30°C

 <b>S1(L-Gly)</b> WT: n.m. TTN M5: 106 TTN WT: n.m. M5: 0.16 ± 0.08 U/mg WT: n.m. con. M5: 0.01 ± 0.004% con.	 <b>S2(L-Ala)</b> WT: 77654 TTN M5: 655398 TTN WT: 116.8 ± 17.8 U/mg M5: 985.9 ± 8.5 U/mg WT: 7.8 ± 2.4% con. M5: 65.5 ± 6.1% con.	 <b>S3(L-Val)</b> WT: 7332 TTN M5: 96929 TTN WT: 37.5 ± 5.7 U/mg M5: 495.8 ± 13.2 U/mg WT: 0.7 ± 0.2% con. M5: 9.7 ± 0.5% con.	 <b>S4(L-Leu)</b> WT: 28266 TTN M5: 124370 TTN WT: 79.7 ± 12.1 U/mg M5: 350.5 ± 4.3 U/mg WT: 2.8 ± 0.3% con. M5: 12.4 ± 1.6% con.	 <b>S5(L-Ile)</b> WT: 14532 TTN M5: 108990 TTN WT: 53.2 ± 8.1 U/mg M5: 398.6 ± 7.8 U/mg WT: 1.5 ± 0.2% con. M5: 10.9 ± 0.4% con.	 <b>S6(L-Met)</b> WT: 56531 TTN M5: 175249 TTN WT: 85.0 ± 12.9 U/mg M5: 263.6 ± 3.2 U/mg WT: 5.7 ± 1.0% con. M5: 17.5 ± 2.1% con.	 <b>S7(L-Cys)</b> WT: 7789 TTN M5: 24924 TTN WT: 39.8 ± 6.1 U/mg M5: 127.5 ± 3.4 U/mg WT: 0.8 ± 0.3% con. M5: 2.5 ± 0.6% con.
 <b>S14(L-Phe)</b> WT: 12528 TTN M5: 144072 TTN WT: 62.0 ± 9.4 U/mg M5: 713.3 ± 11.6 U/mg WT: 1.2 ± 0.4% con. M5: 14.4 ± 2.5% con.	 <b>S13(L-Tyr)</b> WT: 12740 TTN M5: 13122 TTN WT: 63.1 ± 9.6 U/mg M5: 659.5 ± 10.8 U/mg WT: 1.3 ± 0.2% con. M5: 1.4 ± 0.1% con.	 <b>S12(L-Trp)</b> WT: 2763 TTN M5: 17136 TTN WT: 14.1 ± 2.2 U/mg M5: 87.7 ± 6.9 U/mg WT: 0.3 ± 0.3% con. M5: 1.7 ± 0.5% con.	 <b>S11(L-His)</b> WT: 11594 TTN M5: 66663 TTN WT: 42.4 ± 6.3 U/mg M5: 243.8 ± 8.7 U/mg WT: 1.2 ± 0.5% con. M5: 6.7 ± 0.8% con.	 <b>S10(L-Pro)</b> WT: n.m. TTN M5: n.m. TTN WT: n.m. M5: n.m. WT: n.m. con. M5: n.m. con.	 <b>S9(L-Ser)</b> WT: 56529 TTN M5: 169596 TTN WT: 84.6 ± 12.9 U/mg M5: 255.1 ± 4.3 U/mg WT: 5.7 ± 1.2% con. M5: 17.1 ± 1.4% con.	 <b>S8(L-Thr)</b> WT: n.m. TTN M5: 133 TTN WT: n.m. M5: 0.2 ± 0.1 U/mg WT: n.m. con. M5: 0.01 ± 0.003% con.
 <b>S15(L-Asp)</b> WT: 2557 TTN M5: 2763 TTN WT: 13.1 ± 2.0 U/mg M5: 14.1 ± 1.3 U/mg WT: 0.3 ± 0.1% con. M5: 0.4 ± 0.2% con.	 <b>S16(L-Glu)</b> WT: 12339 TTN M5: 30848 TTN WT: 13.1 ± 2.0 U/mg M5: 152.7 ± 2.6 U/mg WT: 1.2 ± 0.4% con. M5: 3.1 ± 0.3% con.	 <b>S17(L-Lys)</b> WT: 12976 TTN M5: 46715 TTN WT: 64.3 ± 9.8 U/mg M5: 231.3 ± 3.6 U/mg WT: 1.3 ± 0.2% con. M5: 4.7 ± 0.6% con.	 <b>S18(L-Arg)</b> WT: 54202 TTN M5: 157187 TTN WT: 81.5 ± 12.4 U/mg M5: 236.5 ± 3.1 U/mg WT: 5.4 ± 0.7% con. M5: 15.7 ± 1.3% con.	 <b>S19(L-Asn)</b> WT: 75403 TTN M5: 625836 TTN WT: 113.4 ± 17.3 U/mg M5: 941.5 ± 8.6 U/mg WT: 7.5 ± 1.2% con. M5: 62.6 ± 2.7% con.	 <b>S20(L-Gln)</b> WT: 12174 TTN M5: 70610 TTN WT: 60.3 ± 9.2 U/mg M5: 349.6 ± 5.8 U/mg WT: 1.2 ± 0.1% con. M5: 7.1 ± 1.4% con.	

<sup>4a</sup>The related performance parameters were determined and calculated by the 2,4-dinitrophenylhydrazine chromogenic method, including TTN, specific activity, and % conversion (black, blue, and green fonts are the TTN<sub>10 min</sub>, specific activity, and % conversion values, respectively). Experimental details and calculation formulas can be found in the [Supporting Information](#), and the parameters of the 24 h reaction are shown in [Table S4](#). n.m. means not measurable. All assays were performed in triplicate, and the data are expressed as mean ± SD.

spectroscopy,<sup>23</sup> ultraviolet photoelectron spectroscopy,<sup>24</sup> photoelectrochemical performance,<sup>25</sup> magnetic resonance spectroscopy,<sup>26</sup> X-ray diffraction,<sup>27</sup> and cryo-electron microscopy.<sup>21</sup> For example, the rate-limiting step (i.e., poor thermostability) of thermostable PET depolymerase was identified through UHPLC monitoring. An automated, high-throughput directed evolution platform was developed to engineer polymer-degrading enzymes, increasing the glass transition temperature ( $T_m$ ) to 82.5 °C.<sup>6</sup> Intelligent computational methods, such as molecular dynamics (MD),<sup>28,29</sup> QM,<sup>18,30–32</sup> density functional theory (DFT),<sup>15,33</sup> kinetic isotope effect calculations,<sup>34</sup> and machine learning,<sup>35</sup> have been developed to determine rate-limiting steps. For example, computational methods have been used to determine the rate-limiting step of reduction amination,<sup>36</sup> carbene,<sup>37</sup> transamination,<sup>30</sup> and other catalytic reactions. QM/MM calculations have been used to reveal that both hydride transfer and C–N cleavage steps are rate-limiting for 3,5-DAHDH, an enzyme that catalyzes reductive amination. Subsequently, a series of variants were rationally engineered, and the activity toward various aliphatic  $\beta$ -amino acids increased by 110–800-

fold without compromising enantioselectivity.<sup>36</sup> This finding demonstrated that hybrid QM calculations and MD simulations can provide a set of efficient, accurate, and powerful tools for elucidating the enzymatic reaction mechanism and relative catalytic efficiency. Utilizing such tools facilitates the development of protein design strategies guided by the catalytic mechanism to achieve desired physical and catalytic properties in enzymes.

A series of  $\alpha$ -keto acids (containing a carboxyl and keto bifunctional group) have been produced by amino acid oxidases through the C–N cleavage reaction. They are widely employed in chemical industries, cosmetics, food, beverages, feed additives, and as components of several drugs against chronic kidney disease.<sup>38–41</sup> L-Amino acid oxidase (LAO) is a flavoenzyme containing noncovalently bound flavin adenine dinucleotide, which catalyzes the stereospecific oxidative deamination of L-amino acids to  $\alpha$ -keto acids, ammonia and H<sub>2</sub>O<sub>2</sub>. Therefore, its potential applications mainly involve the production of  $\alpha$ -keto acids, which are key components of nutrient and ammonia metabolism in the body and used as precursors for synthetic alcohols and unnatural amino acids.

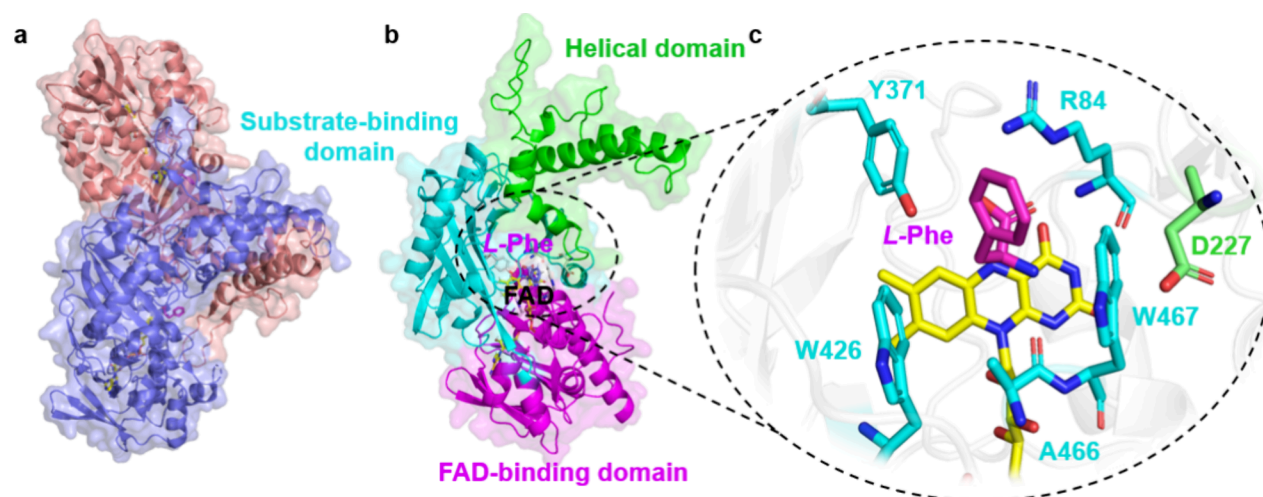


**Figure 1.** Structure of RoLAAO. (a) Structure of dimeric *Rhodococcus opacus* LAAO (PDB ID: 2JB242). Subunit 1 was shown in light blue (chain A of 2JB2) and subunit 2 in salmon (chain B of 2JB2). (b) Three domains of RoLAAO, the substrate-binding domain (residues 52–128, 230–238 and 315–422, cyan); the FAD-binding domain (residues 4–51, 239–314 and 423–488, magentas); helical domain (residues 129–229, green). (c) Close view of the active site of RoLAAO with L-Phe. The cofactor FAD and the L-Phe ligand, R84, D227, Y371, W426, A466, and W467 were shown as stick models colored by elements. The 3D structure of the whole RoLAAO-FAD-L-Phe complex displayed in the surface can be seen in Figure S1b. Also, Figure S1c shows the active site of RoLAAO after rotating a certain angle and the statistical diagram on the distances between the carboxyl group of D227 and the amino group of the substrate (L-Phe) or (aromatic residues, i.e., Y371, W426, or W467).

The L-amino acid oxidase from *Rhodococcus opacus* (RoLAAO, EC 1.4.3.2) belongs to the oxidoreductase family and is characterized by an open substrate binding pocket located between the substrate domain and the cofactor flavin adenine dinucleotide (FAD) domain,<sup>42</sup> which gives it a broad substrate spectrum.<sup>43</sup> However, the low operational catalytic efficiency and substrate specificity are barriers to the industrial application of RoLAAO. Herein, we report a catalytic mechanism-guided protein design strategy to extend the substrate scope and increase the catalytic efficiency of RoLAAO. The catalytic mechanism of RoLAAO was first investigated by structural analysis, MD simulations, and DFT calculations. Then, two barrier steps were identified, and the corresponding protein design strategy was developed. A variant M5 (Y226H/D227H/Y371L/A466C/W467A) with high TTN (96929–175249) toward the selected substrates was achieved by reprogramming the transition states of RoLAAO.

## RESULTS

### Substrate Scope of RoLAAO

To achieve an efficient enzyme to synthesize  $\alpha$ -keto acids from L-amino acids, the enzymes that catalyze C–N cleavage of L-amino acids in the BRENDA Enzyme Database (<https://www.brenda-enzymes.org/>) were classified and screened. A total of 16 enzymes were identified according to the enzyme classification number and were classified according to their substrate range and catalytic characteristics, including transaminases (enzymes 1–2), dehydrogenases (enzymes 3–4), and oxidases (enzymes 5–16). Among these, the reaction catalyzed by transaminase is reversible and requires an excess of amine donors to equilibrate the reaction. L-Amino acid dehydrogenase (LAADH) requires NAD, a costly compound, as a cofactor, as well as complex separation and low catalytic efficiency due to reversible reactions. L-Amino acid deaminase (LAAD) is membrane-dependent oxidase and only suitable for whole-cell conversion, and the inability to reuse LAAD limits its use in industry. Based on substrate scope and enzyme

activity, RoLAAO was selected for further investigation (Table S1). However, when RoLAAO was expressed in *E. coli* BL21, most of it was present in the cell in the form of inclusion bodies. Therefore, soluble mature RoLAAO, MBP-RoLAAO, was obtained by deletion of the original signal peptide maltose-binding protein fusion (Figure S1a).<sup>44</sup> The substrate scope results of MBP-RoLAAO are shown in Table 1. MBP-RoLAAO can catalyze 17 of 20 L-amino acid types (divided into six groups depending on the side chain) with TTNs between 2763 and 77654. For aliphatic amino acids (S1–S5), the highest TTN (77654) was determined for S2, whereas a lower TTN was determined for S3–S5, which did not catalyze S1. For S/O-containing amino acids (S6–S9), TTN values ranged from 7789 to 56531, with the highest TTN determined for S6, whereas MBP-RoLAAO did not catalyze S8. No TTN was determined for the cyclic amino acid S10. For aromatic amino acids (S11–S14), the TTN values ranged from 2763 to 12740, and for acidic amino acids S15 and S16, the TTN values were 2557 and 12339, respectively. For basic amino acids (S17–S20), the TTN values ranged from 12174 to 75403, with the highest TTN determined for S19 (L-Asn). A few D-amino acids (e.g., D-Phe, D-Val, D-Met or D-Leu) were tested, but no relevant activity was detected. We found that the wild type was generally highly active against charged substrates. Furthermore, the TTN values were lower for the substrates of  $\alpha$ -keto acid tablets with important components (detailed descriptions of the components can be found in the Supporting Information), such as S3 (L-Val), S4 (L-Leu), S6 (L-Met), and S14 (L-Phe). The representative substrates (S3, S4, S6, and S14) were selected for further analysis.

### Structure and Catalytic Mechanism of RoLAAO

The crystal structure of RoLAAO in complex with FAD and L-Phe had been solved (PDB ID: 2JB2),<sup>42</sup> but a loop region (432–439) was missing. We applied AlphaFold2<sup>45</sup> to construct a complete structural model of the whole RoLAAO-FAD-L-Phe complex (root-mean-square deviation [RMSD] is only 0.13 Å of all residues C $_{\alpha}$  atoms via structural

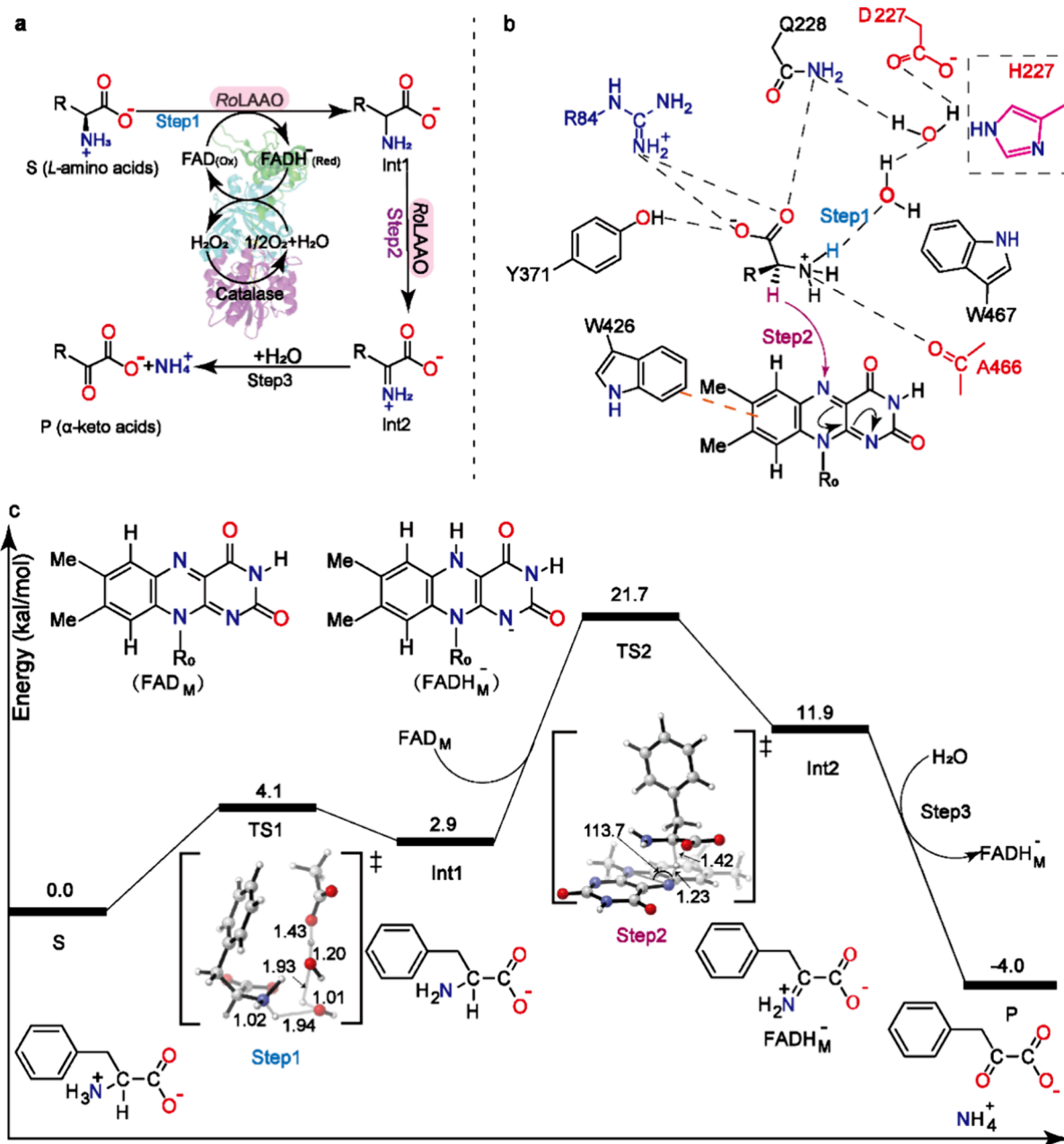


**Figure 2.** Catalytic mechanisms of LAAOs enzyme and computational oxidative deamination pathway of L-Phe. (a) Methods to convert L-amino acids into  $\alpha$ -keto acids. (b) Reaction mechanism for the oxidation of L-amino acids by RoLAAO. (c) DFT-computed Gibbs free energies (in kcal/mol) at the CPCM(water)/B3LYP-D3/6-311++G(2d,p) // CPCM(water)/B3LYP-D3/6-31+G(d) level of theory and transition-state structures (carbon: gray, hydrogen: white, oxygen: red, nitrogen: blue, angles are shown in  $^\circ$ , and distances are shown in Å). The results of direct abstraction of amino proton from substrate by solvent can be seen in Figure S2d. All models were built based on the arrangement of water molecules around the substrate L-Phe in the RoLAAO active site observed from MD simulations (Supporting Information for details). The optimized structure geometries of substrate (S), the intermediates (Int1, Int2), and product (P) of QM cluster models are shown in Figure S2.

alignment with 2JB2) (Figure S1b). RoLAAO is a homodimer (Figure 1a), and each monomer consists of three well-defined domains: a substrate-binding domain (SBD), a FAD-binding domain (FBD), and a helical domain (HD) (Figure 1b). The SBD and FBD generated an open hydrophobic substrate-binding pocket (consisting of R84, Y371, W426, A466, and W467) in the ternary complex structure, the ligand side chain was aligned with the hydrophobic binding pocket, and a FAD isoalloxazine ring was placed at the bottom of the pocket. The HD is exclusively responsible for the unusual dimerization mode of RoLAAO (Figure 1c).

The catalytic mechanisms of the LAAO enzyme are shown in Figure 2a,b, the catalytic mechanism of LAAO include two parts: oxidation half-reaction (OHR) and reduction half-reaction (RHR). For OHR, the reduced FAD is (re)oxidized by  $\text{O}_2$  to yield  $\text{FAD}_{\text{ox}}$  and  $\text{H}_2\text{O}_2$ . For RHR, it generally refers to the process of imino acids formation from corresponding substrate via proton abstraction and hydride transfer. Previous computational studies have shown that the energy barrier of RHR is about 4.4 kcal/mol higher than that of OHR in the catalytic process of amino acid oxidase.<sup>46</sup> In addition, the RHR step is verified as the rate-limiting step by stopped-flow

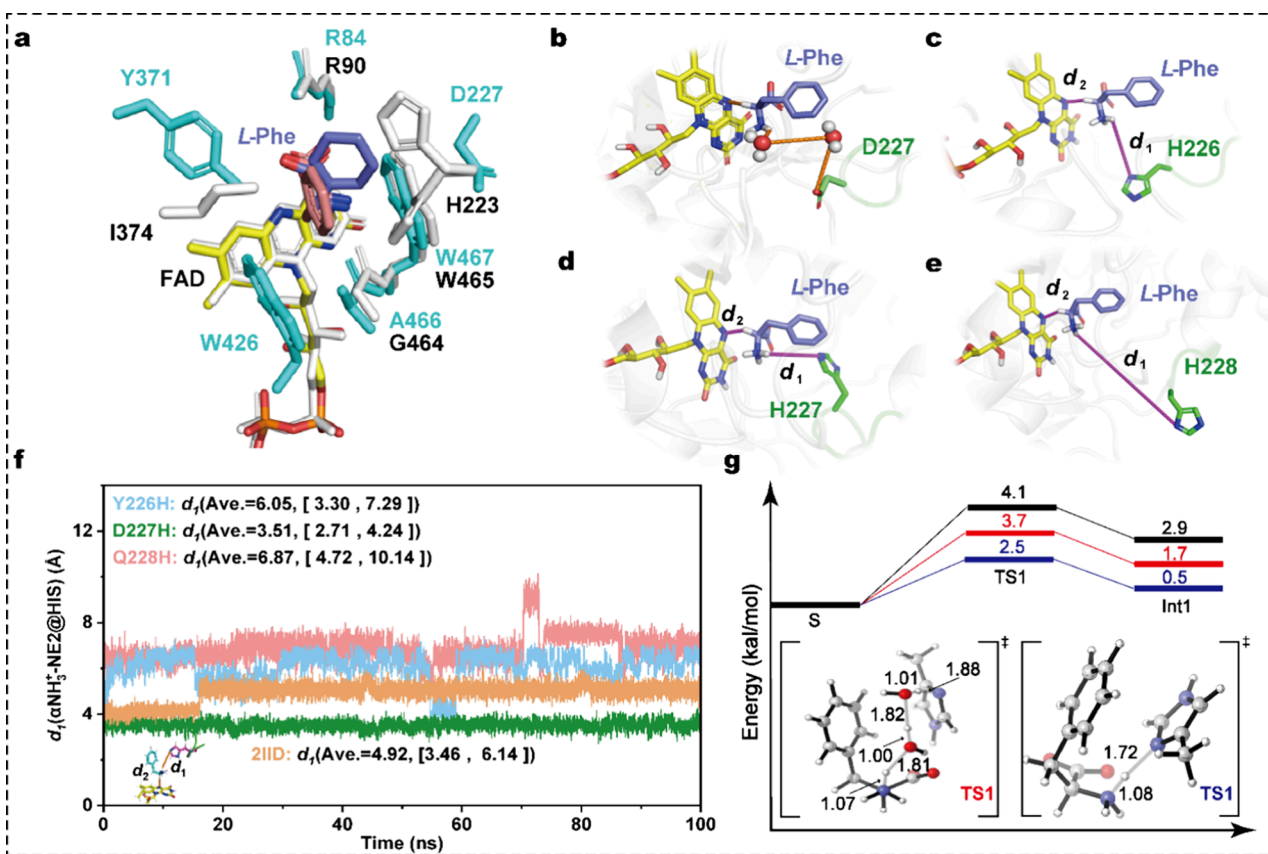


**Figure 3.** Protein engineering and catalytic performance verification of step 1. (a) Structural alignment of RoLAAO-FAD-L-Phe complex (cyan and labels are shown in blue) with CrLAAO from *Calloselasma rhodostoma* (PDB ID: 2IID<sup>48</sup>) (white and labels are shown in black). (b) Transferring H<sup>+</sup> in step 1 of WT. (c–e) Introduction of His residue protein model (Y226H, D227H, and Q228H) using AlphaFold2. (f) Feasibility of three variants verified by MD simulations (2IID (orange), Y226H (light blue color), D227H (green), Q228H (pink)) with the ligand L-Phe. (g) For Step1, DFT-computed Gibbs free energies (in kcal/mol) at the CPCM(water)/B3LYP-D3/6-311++G(2d,p) // CPCM(water)/B3LYP-D3/6-31+G(d) level of theory and transition-state structures (carbon: gray, hydrogen: white, oxygen: red, nitrogen: blue, and distances are shown in Å). All models were built based on the arrangement of water molecules around the substrate L-Phe in the RoLAAO active site observed from MD simulations (Supporting Information for details). The QM cluster models contained S/Int1, imidazole (substitute His), and two H<sub>2</sub>O in step 1 (red line) and contained S/Int1 and imidazole (substitute His) in step 1 (blue line). Also, the optimized structure geometries of these QM cluster models are shown in Figure S4.

experiments, which is consistent with previous reports (additional notes and experimental details can be found in the Supporting Information). Based on these, RHR was comprehensively studied in this manuscript. An overview of the RHR mechanism and the corresponding energy profile of RoLAAO are shown in Figure 2c, where the oxidative deamination reaction in RHR is divided into the following reaction steps. Step 1 is the deprotonation of substrate S (L-amino acids) by two molecules of water and acetate anion, which represent the active water and Asp, respectively, or solvent. A general base (such as Asp) abstracts a proton through active water molecules from the substrate S  $\alpha\text{-NH}_3^+$  (scenario 2) or a proton of substrate S  $\alpha\text{-NH}_3^+$  is abstracted directly through the solvent (scenario 2) to generate the intermediate Int1<sup>42</sup> via the transition state [TS1]. This requires a free activation energy of 4.1/13.1 kcal/mol. In step 2, the C $\alpha$ H (hydride ion: H<sup>-</sup>) of Int1 is transferred to the isoalloxazine ring N5 of the cofactor FAD<sub>M</sub> (FAD<sub>M</sub> is a FAD-truncated model), forming an imino acid Int2 and reduced FAD (FADH<sup>-</sup>)<sup>47</sup> via the transition state [TS2]. This requires the free activation energy of 21.7 kcal/mol, indicating that this reaction can proceed smoothly under enzymatic conditions. Two barrier steps (S  $\rightarrow$  [TS1] (4.1 kcal/mol) in step 1 and

Int1  $\rightarrow$  [TS2] (18.8 kcal/mol) in step 2) were observed (Figure 2c), which reduced the catalytic efficiency of RoLAAO. These results showed that [TS2] was determined to be the rate-limiting step affecting the TTN. In addition, decreasing the Gibbs free energy of [TS1] by increasing the deprotonation of the substrate will accelerate the initiation of reaction. Finally, Int2 is spontaneously hydrolyzed to  $\alpha$ -keto acids in step 3, releasing ammonia, accompanied by the release of 15.9 kcal/mol of energy. Therefore, reducing the energy barriers by reprogramming the transition states [TS1] and [TS2] could be a possible strategy to further increase the catalytic efficiency of RoLAAO.

### Protein Engineering of RoLAAO

In step 1, since the energy barrier of scenario 2 cannot be changed by mutation experiments; thus, we can only enhance the ability to abstract the proton of the substrate amino group by mutating residue D227. When residue D227 and water molecules in the loop region could act as a general base to abstract a proton from the substrate  $\alpha\text{-NH}_3^+$  and generate Int1 (scenario 1). However, this general base was not strongly alkaline, which increased the energy barrier in step 1. There were three general base residues (D, E, and H), with His being the most alkaline residue. Therefore, three His variants, i.e.,

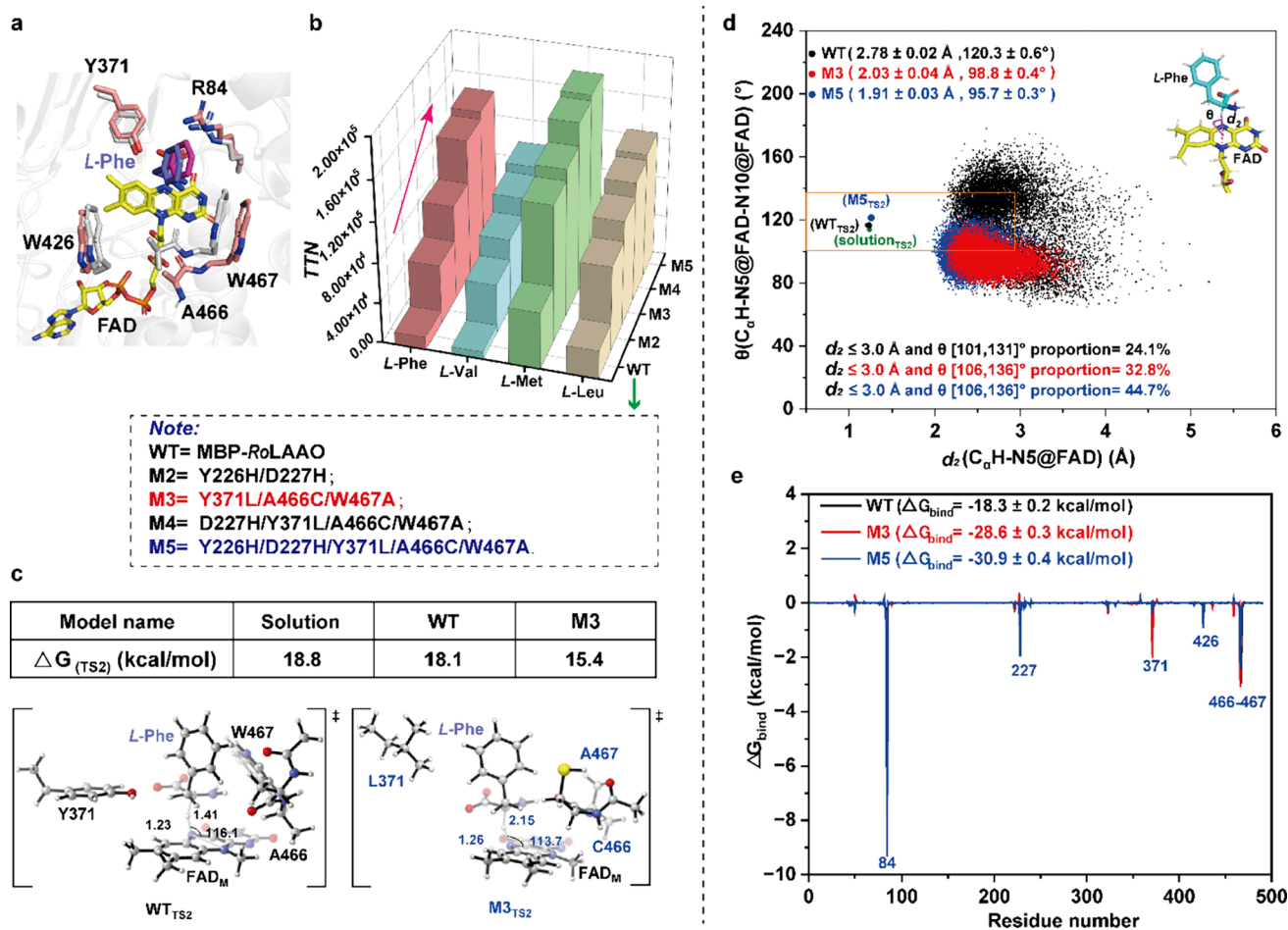


**Figure 4.** Protein engineering and catalytic performance verification of step 1, step 2, and step 1 + 2. (a) Merged [TS2] conformation of the cluster model with the crystal structure of RoLAAO. (b) Oxidative deamination TTN of the RoLAAO wild-type and its variants to the selected substrates. (c) For step 2, DFT-computed Gibbs free energies (in kcal/mol) at the CPCM(water)/B3LYP-D3/6-311++G(2d,p) // CPCM(water)/B3LYP-D3/6-31+G(d) level of theory and transition-state structures (carbon: gray, hydrogen: white, oxygen: red, nitrogen: blue, angles are shown in  $^\circ$ , and distances are shown in  $\text{\AA}$ ). All models were built based on the arrangement of water molecules around the substrate L-Phe in the RoLAAO active site observed from MD simulations (Supporting Information for details). The optimized structure geometries of these QM cluster models are shown in Figure S6. (d) Statistics of catalytic distance ( $d_2$ ) and angle ( $\theta$ ) of ligand L-Phe in WT and variants M3 and M5; (e) Statistics of binding free energy of ligand L-Phe in WT and variants M3 and M5. Data were collected for 4000 snapshots of the last 40 ns MD simulations.

Y226H, D227H, and Q228H, were successfully designed and built at the correct positions (in the region of loop D227) (Figure 3a–e), confirming the feasibility of the three variants (Figure 3f). Furthermore, the transformation experiments showed that three single variants introduced with His residues could increase the TTN for the selected substrates, with the single variant D227H (named M1) and double variant Y226H/D227H (named M2) having the highest TTN (38860–124368 TTN and 48391–135674 TTN, respectively) for the selected substrates (Figure S3a). To confirm further the role of the His residue, residue D227 was mutated to D227A and M2 corresponding to Y226H/D227A, whereas the 227A and Y226H/D227A reduced the TTN by approximately 64.3–88.2 and 30.0–75.1%, respectively, for L-Phe, L-Val, L-Met, and L-Leu, compared with the corresponding value for the WT (Figure S3b).

The high-energy barrier in step 2 was caused by the poor orientation of the substrate to the cofactor FAD. Therefore, the strategies of decrease the energy barrier of step 2 were to adjust the binding orientation of the substrate close to [TS2] by releasing steric hindrance and by strengthening substrate

affinity that is, decreasing the catalytic distance for the transfer of  $\text{H}^-$  between  $\text{C}_\alpha\text{H}$  and  $\text{N5@FAD}$  ( $d_2$ ) and the angle ( $\theta$ ) between the substrate  $\text{C}_\alpha\text{H}$  and the isoalloxazine ring of FAD to be more close to  $d_{2(TS2)}$  and  $\theta_{(TS2)}$ . [TS2] was docked into the active site of the enzyme and performed constrained MD simulations. Five residues (R84, Y371, W426, A466, and W467) that affected the energy barrier in step 2 were identified and are shown in Figure 4a. To reduce steric hindrance, the large-volume residues (R84, Y371, W426, and W467) near the substrate-binding pocket were mutated into a small-volume residue (A) to allow the substrate closer to FAD and obtaining the variants R84A, Y371A, W426A, and W467A. This resulted in a 0.8–1.6-fold and 2.0–3.4-fold increase in the TTNs of the Y371A and W467A variants, respectively, to the selected substrates compared with that of the WT. However, the TTN of variants R84A (forming electrostatic interactions with the carboxyl group of the substrate to recognize the substrate) and W426A (forming  $\pi$ - $\pi$  interactions with the FAD isoalloxazine ring to recognize FAD) to the selected substrates was decreased by 0.56–0.82-fold (Figure S5a). The R- $\pi$  interaction between the substrate side-chain R group and the

Y371 side-chain may influence the approach of the substrate to FAD to affect substrate affinity. Hence, Y371 was mutated as smaller volume residues (L/I/N) with different properties. A very weak interaction between the side chain methyl group of A466 and the substrate side chain may not be conducive to adjusting the substrate side chain posture, thereby affecting substrate affinity. Therefore, A466 was mutated as polar residues (S/T/C) with smaller volumes. Two mutation libraries were then built, and the six variants (Y371L, Y371N, Y371I, A466C, A466E, and A466T) that exhibited higher activity were identified by a screening protocol based on the color reaction of 2,4-dinitrophenylhydrazine with the product  $\alpha$ -keto acids (Figure S5b).<sup>47,49</sup> Two rounds of iterative mutagenesis were performed to obtain a triple variant M3 (Y371L/A466C/W467A) (Figure S5 and Figure 4b), and TTN increased by 2.6–9.4-fold compared with that of the WT for the selected substrates.

Finally, variant M3 (Y371L/A466C/W467A) was used as a template and mutated in combination with mutants M1 (D227H) and M2 (Y226H/D227H) to obtain variants M4 (D227H/Y371L/A466C/W467A) and M5 (Y226H/D227H/Y371L/A466C/W467A), respectively (Figure 4b). Variant M5 showed a 3.1–13.1-fold increase in the TTN, with the highest value observed for the oxidative deamination of L-Met (175249 TTN) and the greatest improvement for L-Phe (144072 TTN). Variant M5 showed a lower  $K_m$  than the WT. These correspond to 2.4-, 6.3-, 2.9-, and 3.7-fold reductions in  $K_m$  for the substrates L-Phe, L-Val, L-Met, and L-Leu in comparison to WT, indicating that the mutagenesis of M5 favors the binding of these substrates (Figure 4b and Table S2). Moreover, the  $k_{cat}$  values of variant M5 were 240.16 (L-Phe), 158.84 (L-Val), 296.53 (L-Met), and 205.02 s<sup>-1</sup> (L-Leu), which are 11.5, 13.1, 3.1, and 4.4 times higher, respectively, than those of the WT. As a result,  $k_{cat}/K_m$  of variant M5 increased by 28.1-, 82.8-, 9.2-, and 16.4-fold.

### Analysis of Performance Enhancement Mechanisms for RoLAAO

The 3D structure of the M1/M2/M3/M5-FAD-L-Phe complex was constituted by hybrid MD simulations and DFT calculations. The results showed that (1) the RMSD values of M1, M2, M3, and M5 were 0.12, 0.12, 0.13, and 0.52 Å, respectively, indicating that mutagenesis in the active pocket did not considerably alter the overall structure of RoLAAO (Figure S9a). (2) For M1 or M2 in step 1, the distance for proton transfer between  $\alpha$ -NH<sub>3</sub><sup>+</sup> and N@His (called  $d_{1(\text{His models})}$ ) was >3 Å but close to  $d_{1(2IID)}$  (Figure 3f), which was consistent with what was observed in CrLAAO (PDB ID: 2IID);<sup>48</sup> the His residue acted as a general base and transferred a proton from the substrate  $\alpha$ -NH<sub>3</sub><sup>+</sup> to generate Int1. (3) The introduced His residue replacing a general base could increase the efficiency of H<sup>+</sup> transfer, leading to a decrease in the energy barrier of step 1 (S → [TS1]) from 4.1 kcal/mol (in the WT) to 2.5–3.7 kcal/mol (Figure 3g).

For the variants M3 and M5, the energy barrier of step 2<sub>M3</sub> (Int1 → [TS2]) decreased from 18.8 (of the WT) to 15.4 kcal/mol (Figure 4c), favoring the C<sub>α</sub>H (hydride ion: H<sup>-</sup>) transfer of substrate. This occurred because the M3 and M5 variants simultaneously stabilized the transition state and destabilized the ground state and increased the proportion of the catalytic active conformation by a shorter  $d_2$  and a more appropriate  $\theta$  to the model substrate (L-Phe), compared with those of the WT (Figure 4d): (1) the  $d_2$  of variants M3 and

M5 was 2.03 and 1.91 Å, which were 0.75 and 0.87 Å shorter than that of the WT (2.78 Å), respectively. (2) A significant change in the  $\theta$  (98.8 and 95.7°, respectively) of variants M3 and M5, which was 21.5 and 24.6° lower, respectively, than that of the WT (120.3°). (3) The  $d_2$  and  $\theta$  values were closely to  $d_{2(\text{TS2})}$  and  $\theta_{(\text{TS2})}$ , respectively. The distance of the C<sub>α</sub>H transfer  $d_2 \leq 3$  Å and  $\theta$  (106, 136°) ( $\theta_{(\text{TS2})}$  can vary by 15°) of the variants M3 and M5 were determined to be 32.76 and 44.79%, which were 8.74 and 20.77% higher, respectively, than that of the WT (24.02%). (4) The binding free energy ( $\Delta G_{\text{bind}}$ ) of the variants M3 and M5 was higher than that of the WT (-18.3 kcal/mol) due to the enhanced interaction (Figure 4e).

### Substrate Scope of RoLAAO and Its Applications in the Synthesis of $\alpha$ -Keto Acids

As shown in Table 1, the variant M5 can transform 19 of the 20 kinds of L-amino acids to the corresponding keto acids, showing modest-to-excellent catalytic efficiency (TTNs varied from 106 to 655398). For S1–S5, M5 showed a higher TTN than the WT (4.4–13.5-fold), except for S1 (TTN from 0 to 106), with the highest TTN in S2 (655398). For S6–S9, TTN was increased approximately 3-fold compared with that of the WT, except for S8 (TTN from 0 to 133). However, variant M5 did not exhibit catalytic activity for S10, which is a cyclic amino acid. For S11–S14, TTN was increased by 5.7–11.5-fold and 1.1–2.5-fold for S15 and S16, respectively, compared with that of the WT. For S17–S20, TTN was increased by 2.9–8.3-fold compared with that of the WT. So M5 was an efficient universal enzyme, showing a broad substrate spectrum and a high catalytic efficiency for L-amino acids.

To further increase the efficiency of the production of  $\alpha$ -keto acids, the transformation conditions were optimized using *E. coli* as a whole-cell catalyst expressing the variant M5 (Figure S7). The reactions were then scaled to a 5 L reactor under the optimum conditions (pH 8.0 Tris-HCl, 30 °C, 20 g/L wet cell, and 2200 U/mL catalase). The titer of  $\alpha$ -keto acids ( $\alpha$ -phenylpyruvic acid [ $\alpha$ -PPA],  $\alpha$ -keto-isovalerate [ $\alpha$ -KIV],  $\alpha$ -keto- $\gamma$ -methylthiobutyric acid [ $\alpha$ -KMTB], and  $\alpha$ -ketoisocaproate [ $\alpha$ -KIC]) produced from 100 g/L of the corresponding substrates (L-Phe, L-Val, L-Met, or L-Leu) was  $\geq 95.1$  g/L with  $\geq 95\%$  conversion yield and  $\geq 142.7$  g/L/d space-time yields (STY) in 12–24 h. These findings demonstrate the potential of the engineered variant M5 to produce  $\alpha$ -keto acids ( $\alpha$ -PPA,  $\alpha$ -KIV,  $\alpha$ -KMTB, and  $\alpha$ -KIC) from L-amino acids for industrial applications due to high titers and high conversion rates.

## DISCUSSION

In this study, a C–N cleavage enzyme RoLAAO was screened to efficiently produce  $\alpha$ -keto acids from L-amino acids. Also, two key steps, S → [TS1] in step 1 and Int1 → [TS2] in step 2 were identified based on the catalytic mechanisms via MD simulation and DFT calculations. We used rational design (reprogramming the [TS1] and [TS2] transition states to reduce the energy barrier) to engineer the variant M5 with the highest TTN. The substrate spectrum of variant M5 expanded to 19 types of L-amino acids with high TTN, and the titer and conversion rate of  $\alpha$ -keto acids were 95.1 g/L and 95%, respectively, in a 5 L bioreactor. These results demonstrate that lowering the energy barrier of RoLAAO is a potential strategy to further increase catalytic efficiency. These results demonstrate that lowering the energy barrier of RoLAAO is a potential strategy to further increase catalytic efficiency. Also,

these findings demonstrate the efficacy of the developed variant M5 for improving the  $\alpha$ -keto acids titer and represent a potentially attractive strategy for the industrial production of  $\alpha$ -keto acids from L-amino acids. This successful engineering effort could potentially guide protein engineering on other enzymes to improve their catalytic efficiency.

In this study, two transition states ([TS1] and [TS2]) were identified. [TS2] was determined to be the rate-limiting step affecting the TTN by combining the catalytic mechanism of LAAO with QM and MD tools. The rate-limiting step in LAAO is similar to the C–N cleavage reaction catalyzed by LAAD<sup>47</sup> because both enzymes are dependent on FAD, and their rate-limiting step involves an energy barrier caused by hydride transfer. However, this differs from C–N cleavage catalyzed by transaminases, such as PLP-dependent  $\omega$ -transaminase, which has more rate-limiting steps.<sup>30</sup> In our study, based on the catalytic mechanism, the energy barrier was reduced by reprogramming [TS1] and [TS2]. Thus, the M5 variant led to a significant increase in the TTN (1.5–26.8-fold increase for the selected substrates). Rational enzyme design based on catalytic mechanisms has been widely used to modify enzymes, such as the coronavirus 3C-like protease (3CL<sup>Pro</sup>),<sup>50</sup> tryptophan 6-halogenase (Thal),<sup>51</sup> cytochrome C,<sup>37</sup> and imine reductase,<sup>52</sup> to meet the requirements of industrial application. For example, after determining the catalytic mechanism of 3CL<sup>Pro</sup>, a residue pair (Glu–His) and a stable hydrogen bond were found to play a substrate-binding role, and a partial negative charge cluster formed by Arg–Tyr–Asp was found to be essential for catalysis. Following a mutation strategy (i.e., introducing a powerful hydrogen bond interaction between the ligand and critical residue of 3CL<sup>Pro</sup>), the enzymatic activity was improved by 8-fold.<sup>50</sup> In addition, enzyme energy barrier engineering has been used to improve the physical and catalytic properties of  $\omega$ -transaminase ( $\omega$ -TA)<sup>30</sup> and decarboxylase.<sup>32</sup> For example, the catalytic efficiency for bulky substrates was increased by 1.5–26.8-fold in turnover number by decreasing the energy barrier of three high-energy barrier steps in  $\omega$ -TA.<sup>30</sup> Another example is the reduction in the energy barrier of orotidine-5'-monophosphate decarboxylase by creating an unstable ground state of the substrate, which resulted in a considerable increase rate of 17 orders of magnitude compared with that of the uncatalyzed reaction.<sup>32</sup> The catalytic mechanism-based protein design strategy exhibits several advantages, including small mutation libraries, high accuracy, and a high success rate, which could greatly reduce the required experimental effort within reasonable limits.

$\alpha$ -Keto acids can be produced from the corresponding L-amino acids by the catalytic activity of transaminase,<sup>30</sup> LAAD,<sup>47</sup> LAAO,<sup>42,43,48</sup> and L-glutamate oxidase (LGOX).<sup>53</sup> Among these, the reaction catalyzed by transaminase is reversible and requires many amine donors.<sup>30</sup> LAAD is a membrane-dependent and only suitable for whole-cell conversion,<sup>47</sup> the conversion efficiency of the pure enzyme is very low, and it cannot be immobilized. LGOX can only catalyze ketoglutarate from glutamate due to its high specificity,<sup>53</sup> such as for the production of  $\alpha$ -ketoglutarate, which has been shown in the industrial scale (LGOX was applied with a substrate concentration of 73.6 g/L (339 mM) and reached a space-time yield of 14.2 g/L/h).<sup>54</sup> In recent years, a multitude of studies have focused on engineering enzymes that catalyze the C–N cleavage of L-amino acids to produce  $\alpha$ -keto acids. For instance, the strategy of engineering

substrate pockets and channels is used to design LAAD's pocket and channel; for the substrates, L-Leu and L-Ile significantly improved the catalytic efficiency of  $\alpha$ -ketoisocaproate (yield 107.1 g/L, conversion 98.0%) and  $\alpha$ -keto- $\beta$ -methylvalerate (yield 98.9 g/L, conversion 99.0%).<sup>55</sup> Another study revealed that shortening the hydride transfer distance and expanding the substrate spectrum of LAAD can efficiently catalyze the oxidative deamination of six L-amino acids to directly synthesize  $\alpha$ -keto acids.<sup>47</sup> However, it was difficult for these engineering enzymes to use one of them to catalyze the synthesis of various  $\alpha$ -keto acids via C–N cleavage of L-amino acids. Therefore, LAAO is the most suitable enzyme for the synthesis of a series of  $\alpha$ -keto acids. In this study, the best variant, M5, could catalyze six groups and 20 kinds of natural L-amino acids, and the catalytic performance for S1–S20 was increased from a TTN of approximately to approximately 655398, except that for S10. The M5 variant was able to convert a series of L-amino acids into their corresponding  $\alpha$ -keto acids. It is an efficient universal enzyme, showing a broad substrate spectrum and a high catalytic efficiency for L-amino acids. The M5 variant developed in this study can be used to produce  $\alpha$ -keto acids ( $\alpha$ -PPA,  $\alpha$ -KIV,  $\alpha$ -KMTB, and  $\alpha$ -KIC) at high titers and with high conversion rates, which could be used to treat nephropathy. The results of our study show that RoLAAO is an excellent enzyme for the industrial production of  $\alpha$ -keto acids.

## CONCLUSIONS

In conclusion, a C–N cleavage enzyme RoLAAO was screened to efficiently produce  $\alpha$ -keto acids from L-amino acids. Also, two key steps, S  $\rightarrow$  [TS1] in step 1 and Int1  $\rightarrow$  [TS2] in step 2, were identified based on the catalytic mechanisms via MD simulation and DFT calculations. We then developed a protein engineering strategy to reprogram the [TS1] and [TS2] transition states to reduce the energy barrier, and a variant M5 with the highest TTN was achieved. The substrate spectrum of variant M5 expanded to 19 types of L-amino acids with high TTN, and the titer and conversion rate of  $\alpha$ -keto acids were 95.1 g/L and 95%, respectively, in a 5 L bioreactor. These results demonstrate that lowering the energy barrier of RoLAAO is a potential strategy to further increase catalytic efficiency. Also, these findings demonstrate the efficacy of the developed variant M5 for improving the  $\alpha$ -keto acids titer and represent a potentially attractive strategy for the industrial production of  $\alpha$ -keto acids from L-amino acids. This successful engineering effort could potentially guide protein engineering on other enzymes to improve their catalytic efficiency.

## METHODS

### Materials

The expression plasmid pET-28a (+) and host strain *E. coli* BL21 (DE3) were purchased from Novagen (Madison, WI, USA). The construct containing the MBP tag strain, pET-28a-Sr<sub>MBP</sub>PLD/BL21(DE3),<sup>44</sup> was obtained from the FMME laboratory (Jiangnan University, China). The restriction enzymes (*Bam*H I, *Hind* III, and *Dpn* I), Prime STAR Max DNA polymerase, and KOD polymerase, were purchased from TaKaRa Biomedical Technology (Dalian, China), and a one-step cloning kit was supplied by Vazyme (Nanjing, China). The cloning inserts were generated via the polymerase chain reaction (PCR) of the open reading frames (ORFs) of interest from the respective genomes or synthesized by GENEWIZ (Suzhou, China). Except for the wild type of RoLAAO synthesized by GENEWIZ, MBP-RoLAAO and variants were obtained from plasmids

of existing strains in the laboratory; the DNA and protein sequences can be seen in the [Supporting Information](#). Catalase, isopropyl  $\beta$ -D-1-thiogalactopyranoside (IPTG), and the required antibiotics were purchased from BBI Life Sciences (Shanghai, China). L-Amino acids were purchased from Aladdin Reagents (Shanghai, China). Product  $\alpha$ -keto acid standards were purchased from Sigma-Aldrich (St. Louis, MO, USA). Other commercial reagents were purchased from Sinopharm Chemical Reagent (Shanghai, China) and used without further purification. All other chemicals and solvents were purchased commercially.

### Enzyme Selection, Screening, Expression, and Purification

To identify an efficient enzyme for the synthesis of  $\alpha$ -keto acids from L-amino acids, we screened and selected enzymes that catalyze the cleavage of C–N bonds of L-amino acids from the BRENDA Enzyme Database (<https://www.brenda-enzymes.org/>). Among them, transaminases (enzymes 1–2) catalyzing transamination require additional amino acceptors (e.g.,  $\alpha$ -ketoglutaric acid); the dehydrogenase (enzymes 3–4)-catalyzed reaction is reversible and requires the addition of the cofactor NAD. Oxidases could be divided into broad-spectrum oxidases (enzyme 5) and specialized oxidases (enzymes 6–16) ([Table S1a](#)). Generally, broad-spectrum amino acid oxidases (EC 1.4.3.2) can act on a variety of substrates, whereas specialized oxidases act only on their corresponding substrate amino acids and their derivatives. Using EC 1.4.3.2 as the keyword, a total of 228 LAAOs from different organisms were found, of which most were of eukaryotic origin (62.99%), with the viperus source as the widest specificity of substrates; it acted on a variety of amino acid substrates ([Table S1b](#)). Among them, LAAOs from fungi and cyanobacteria have a narrower substrate spectrum, catalyzing reactions involving up to 4–5 substrates, and these LAAOs are not easily expressed in soluble form in *E. coli*. Hence, LAAO derived from bacteria were screened in detail according to the catalytic substrates of LAAO, and the results are shown in [Table S1c](#). Among them, an LAAO from *Rhodococcus opacus* (RoLAAO) with a broad substrate scope was screened as the research target.

All the desired purified proteins and variants were subjected to the following operating conditions: strains were cultivated in LB medium containing 0.05 mg/mL kanamycin at 220 rpm and 37 °C for 8–12 h and used as the inoculum (2%). The culture was then transferred to Terrific Broth medium with appropriate kanamycin and cultured at 37 °C and 220 rpm. When the OD<sub>600</sub> of the culture broth reached 0.6–0.8, IPTG at a final concentration of 0.2 nM was added to the medium. The cells were induced at 16 °C for 18 h. After induction with IPTG, the medium was centrifuged at 6000  $\times$  g, 4 °C for 10 min; the cells were collected and then resuspended in a lysis buffer (20 mM Tris-HCl at pH 8.0, 20 mM imidazole, and 500 mM NaCl); and the cells were lysed using a high-pressure homogenizer. The resulting crude lysate was centrifuged at 40,000  $\times$  g at 4 °C for 30 min. The supernatant was collected, and the protein containing the His-tag was captured using a Ni-NTA Superflow resin for 30 min and then released using an elution buffer (20 mM Tris-HCl at pH 8.0, 0.3 M NaCl, and 0.5 M imidazole). Protein concentration was determined using a bicinchoninic acid protein assay kit (Solarbio, China), and purity was determined using sodium dodecyl-sulfate polyacrylamide gel electrophoresis.

### Mutagenesis Experiments

The experiments about protein engineering of RoLAAO were performed using whole-plasmid PCR with KOD-Plus-Neo. The whole plasmid PCR system (50  $\mu$ L) was composed of KOD DNA polymerase (1  $\mu$ L), 10  $\times$  KOD PCR Buffer (5  $\mu$ L), 2 mM dNTP mix (5  $\mu$ L), 25 mM MgSO<sub>4</sub> (3  $\mu$ L), template (50–200 ng), corresponding primers (10  $\mu$ M with 1  $\mu$ L), and sterilized water. The PCR product was digested with the *DpnI* quick-cutting enzyme at 37 °C for 30–45 min. The PCR products were transformed into *E. coli* BL21 (DE3) cells for the following screening or DNA sequencing (GENEWIZ, China). Details of the mutagenesis experiments can be found in the [Supporting Information](#), the primers used are listed in [Table S3](#).

### Performance Parameter Assay

The performance parameters of RoLAAO was monitored using the 2,4-dinitrophenylhydrazine chromogenic method. The principle is that the products  $\alpha$ -keto acids and 2,4-dinitrophenylhydrazine will undergo a color development reaction to produce brownish-red 2,4-dinitrophenylhydrazone.

### Analytical Methods of Substrate L-Amino Acids and Product $\alpha$ -Keto Acids

The samples were filtered through a 0.22  $\mu$ m organic membrane, and then the titer of substrate L-amino acids was determined via HPLC using a Dionex UltiMate 3000 VWD detector (Thermo Fischer Scientific, Germany), an Agilent Zorbax SB-Aq column (4.6  $\times$  150 mm; Agilent Technologies, USA), and an FLD detector (Thermo Fischer Scientific, Germany) under the following conditions: excitation at 330 nm and emission at 465 nm, automatic precolumn derivatization with o-phthalaldehyde (OPA), sample injection volume of 8  $\mu$ L, sample mixed with 4  $\mu$ L of OPA, a flow rate of 1 mL/min, and mobile phase A consisting of a buffer (10 mM KH<sub>2</sub>PO<sub>4</sub> at pH 5.3), methanol, and acetonitrile at 1:3:5 (v/v/v). The gradient was applied as follows: 80% A at 0 min, 65% A at 5 min, 35% A at 10 min, 30% A at 15 min, 50% A at 20 min, and 80% A at 23 min.

The titer of  $\alpha$ -keto acids was determined via HPLC using a Dionex UltiMate 3000 VWD detector and an Aminex HPX-87H Ion Exclusion column (300  $\times$  7.8 mm) under the following conditions: column temperature of 35 °C, detection wavelength of 210 nm, injection volume of 10  $\mu$ L, and flow rate of 0.6 mL/min. The mobile phase consisted of 5 mM H<sub>2</sub>SO<sub>4</sub>. The HPLC chromatogram of the substrate/product standard sample and the corresponding conversion of the sample solution are shown in [Figures S10–S25](#). The conversion of  $\alpha$ -keto acids from L-amino acids was calculated as follows: conversion = [(m1/M1)  $\div$  (m2/M2)]  $\times$  100%. In the formula, the molecule m1 is the mass of the product  $\alpha$ -keto acids, the denominator m2 is the mass of the substrate L-amino acids, M1 represents the relative molecular mass of the substrate, and M2 represents the relative molecular mass of the product.

### Initial Structural Preparation for Computational Studies

The initial structure of RoLAAO with bound cofactor FAD and L-Phe was based on the structure of RoLAAO (PDB ID: 2JB2).<sup>42</sup> The missing residues (432–439) in the crystal structure of 2JB2 were completed using AlphaFold2, and then the entire RoLAAO structure was created by structural alignment with 2JB2. The initial coordinates of the RoLAAO variants were constructed using AlphaFold2 (See "*ab initio modeling of RoLAAO with AlphaFold2*" for details in [Supporting Information](#)). The protonation states of the charged residues were determined at a constant pH of 8.0, based on *pK<sub>a</sub>* calculations using the PROPKA program<sup>56</sup> and considering the local hydrogen bonding network. In the RoLAAO wild-type/variant M3 models, residues His13, 296, 400, and 436 were set as HIE, and residues His76, 89, 385, 460, 469, 481, and 483 were set as HID. In the models of the histidine-containing RoLAAO variant, residues His13, 296, 400, and 436 were assigned as HIE, residues His76, 89, 385, 460, 469, 481, and 483 were set as HID, and the histidine mutation site was set as either HID or HIE. In the models of 2IID, residues His35, 57, 223, and 440 were set as HIE, and residues His256, 314, 321, 342, 360, 401, and 463 were set as HID. In these models, all Asp and Glu residues were deprotonated, while the Lys and Arg residues were protonated. The bond and angle force constants were determined using the Seminario method,<sup>57</sup> and point charge parameters for electrostatic potentials were determined using the ChgModB method. Each model was neutralized by the addition of Na<sup>+</sup> ions and solvation in a truncated octahedral TIP3P water box with a buffer distance of 10 Å on each side.

### Molecular Docking

To dock the FAD cofactor and L-Phe to the active sites of the RoLAAO variants, 50000 uniformly distributed snapshots from the 100 ns MD simulation (with time intervals of 2 ps) were selected and divided into 10 groups using a hierarchical agglomerative (bottom-

up) approach. The cofactor FAD and substrate L-Phe of RoLAAO were fully optimized at the b3lyp/6-311++g(2d,p) level of Gaussian 16 using the CPCM model in water.<sup>58</sup> FAD positions were determined by alignment with the 2JB2 structure, and then the substrate L-Phe was docked to the active site of one representative group snapshot to mimic the FAD-L-Phe-RoLAAO complex. Molecular docking was performed with the Lamarckian genetic algorithm local search method using AutoDock Vina.<sup>59</sup> The docking approach was used for a rigid receptor conformation, while all rotatable torsion bonds of L-Phe were left free. A grid box was centered near the residues 84, 371, 426, 466, and 467 and FAD isoalloxazine ring, and its size was set at 20 × 20 × 20 Å with a spacing of 0.375 Å. A total of 500 independent docking runs were performed with a maximum energy evaluation of 2.5 × 10<sup>7</sup>. The 500 docked conformations obtained were clustered with an RMSD of 2.0 Å and ranked using an energy-based scoring function. The possible catalytically active binding modes were selected as initial configurations to perform MD simulations of RoLAAO variants in complex with FAD-L-Phe, according to the scoring function and reasonable conformation.

### MD Simulations

All MD simulations were performed using the Amber 18 package software.<sup>60</sup> The MD pre-equilibrated RoLAAO wild-type, its variants, 2IID structures, and possible catalytically active binding modes of FAD and L-Phe were used as initial conformations for MD simulations of the protein–ligand complexes. The partial charges of FAD and L-Phe were fitted using HF/6-31G(d) calculations and the restrained electrostatic potential protocol<sup>61</sup> implemented by the Antechamber module in the Amber 18 package.<sup>60</sup> The force field parameters for FAD and L-Phe were adapted from the standard general amber force field 2.0 (gaff2) parameters,<sup>62</sup> whereas the standard Amber14SB force field was used to describe the protein. Each system was first neutralized with Na<sup>+</sup> counterions and solvated with explicit TIP3P water in a truncated octahedral box with a 10 Å buffer distance. The resulting system contained 492 (RoLAAO wild-type [or its variants] bound with FAD and L-Phe) and 485 (2IID bound with FAD and L-Phe) residues/molecules.

Each system was brought to equilibrium with a series of minimizations interspersed by short MD simulations, during which restraints on the heavy atoms of the protein backbone were gradually released (with force constants of 10, 2, 0.1, and 0 kcal [mol Å<sup>-2</sup>]) and then slowly heated from 0 to 300 K for 50 ps. Finally, a standard unrestrained 100 ns MD simulation with periodic boundary conditions at 300 K and 1 atm was performed. The pressure was maintained at 1 atm and coupled with isotropic position scaling. The temperature was maintained at 300 K using the Berendsen thermostat. Long-range electrostatic interactions were treated using the particle mesh Ewald method, and a cutoff of 12 Å was applied to both particle mesh Ewald and van der Waals interactions.<sup>63</sup> A time step of 2 fs was used along with the SHAKE algorithm for hydrogen atoms, and a periodic boundary condition was used. For each system, total of three replicas of 100 ns each were carried out, accumulating a total of 300 ns of simulation time. The conformations visited by the enzyme along all this simulation time were clustered based on protein backbone RMSD, and the most populated cluster was selected as a representative structure of these enzymes. The CPPTRAJ module was used to calculate the stability (structure, energy, and temperature variations), convergence (RMSD of the structures), distance, and angle of each system in the AmberTools18 software.<sup>60</sup>

### DFT Calculations

DFT calculations were performed using the Gaussian 16 package.<sup>64</sup> All DFT structures were constructed based on the crystal structure of RoLAAO (PDB ID: 2JB2), the results of MD simulations, and the catalytic mechanism (see section “Additional Notes on Computational Modeling” of the Supporting Information for details). Considering the characteristics of the results of RoLAAO in our study, the catalytic site is located in the open active pocket, and its dielectric constant is consistent with the CPCM model. In addition, this model is also used in many calculation models of direct contact between active sites and aqueous solution. Therefore, we used a

continuum model (CPCM)<sup>65–68</sup> that simulates the system being completely surrounded by liquid water and is suitable for a reaction taking place inside the pocket of an enzyme. Geometry optimizations of the minima and transition states involved were performed at the B3LYP-D3 level of theory with the 6-31+G (d) basis set. Vibrational frequency calculations were performed at the same level to ensure that all stationary points were transition states (one imaginary frequency) or minima (no imaginary frequency) and to evaluate zero-point vibrational energies and thermal corrections at 298 K. Single-point energy calculations were performed at the B3LYP-D3 level using the 6-31+G(2d,p) basis set. Solvation by water was considered using the CPCM model<sup>68</sup> for all of the above calculations. Additional notes on computational modeling and all supporting computational data can be found in the Supporting Information. Optimized DFT structures are illustrated with CYLView (<https://www.cylview.org/>).

## ■ ASSOCIATED CONTENT

### Supporting Information

The Supporting Information is available free of charge at <https://pubs.acs.org/doi/10.1021/jacsau.3c00672>.

Additional experimental information and procedures including the DNA sequence and protein sequence, details of the mutagenesis experiments, details of the performance parameters assay, process for ab initio modeling of RoLAAO with AlphaFold2, additional notes on computational modeling, rate-limiting step verification experiments, HPLC chromatograms, HRMS spectrum, <sup>1</sup>H NMR spectra, and <sup>13</sup>C NMR spectra for substrates and products and all supporting tables (Table S1–S3); all supporting figures (Figures S1–S29), and supporting computational data (PDF)

## ■ AUTHOR INFORMATION

### Corresponding Author

**Jing Wu** – School of Life Sciences and Health Engineering, Jiangnan University, Wuxi 214122, China; Phone: +86-510-85910059; Email: [wujing@jiangnan.edu.cn](mailto:wujing@jiangnan.edu.cn); Fax: +86-510-85910059

### Authors

**Yaoyun Wu** – School of Life Sciences and Health Engineering, State Key Laboratory of Food Science and Resources, and School of Biotechnology, Jiangnan University, Wuxi 214122, China; [orcid.org/0000-0002-4491-3923](https://orcid.org/0000-0002-4491-3923)

**Yaozhong Cui** – Jiangsu Xishan Senior High School, Wuxi 214174, China

**Wei Song** – School of Life Sciences and Health Engineering, Jiangnan University, Wuxi 214122, China; [orcid.org/0000-0002-2278-2205](https://orcid.org/0000-0002-2278-2205)

**Wanqing Wei** – State Key Laboratory of Food Science and Resources, Jiangnan University, Wuxi 214122, China

**Zhizhen He** – School of Life Sciences and Health Engineering, Jiangnan University, Wuxi 214122, China

**Jinyang Tao** – School of Life Sciences and Health Engineering, Jiangnan University, Wuxi 214122, China

**Dejing Yin** – School of Biotechnology, Jiangnan University, Wuxi 214122, China

**Xiulai Chen** – State Key Laboratory of Food Science and Resources, Jiangnan University, Wuxi 214122, China;

[orcid.org/0000-0002-9749-4558](https://orcid.org/0000-0002-9749-4558)

**Cong Gao** – State Key Laboratory of Food Science and Resources, Jiangnan University, Wuxi 214122, China;

[orcid.org/0000-0001-8505-2026](https://orcid.org/0000-0001-8505-2026)

Jia Liu – State Key Laboratory of Food Science and Resources, Jiangnan University, Wuxi 214122, China  
Liming Liu – State Key Laboratory of Food Science and Resources, Jiangnan University, Wuxi 214122, China

Complete contact information is available at:  
<https://pubs.acs.org/10.1021/jacsau.3c00672>

### Author Contributions

Y.W. and J.W. conceived the study and designed the experiments. Y.W., Z.H. and J.T. performed all experiments. Y.W. and W.W. performed computational studies on protein dynamics. D.Y. performed the X-ray diffraction. X.C., C.G., and J.L. provided technical assistance. W.S., W.W., L.L., and J.W. provided overall project supervision. Y.W. analyzed the data and wrote the manuscript. All authors read, edited, and approved the final manuscript. CRediT: **Yaoyun Wu** data curation, funding acquisition, methodology, software, writing-original draft, writing-review & editing; **Yaoyun Wu** methodology; **Wanqing Wei** software; **Zhizhen He** data curation, formal analysis; **Jinyang Tao** methodology; **Dejing Yin** software; **Xiulai Chen** writing-review & editing; **Cong Gao** writing-review & editing; **jia liu** writing-review & editing; **Liming Liu** writing-review & editing; **Jing Wu** writing-original draft, writing-review & editing.

### Funding

The National Key R&D Program of China (grant no. 2021YFC2100100), the General Program of National Natural Science Foundation of China (grant no. 22178146), and the Key R&D Program of Jiangsu Province (grant no. BE2020341-1), Postgraduate Research&Practice Innovation Program of Jiangsu Province (grant no. KVCX22\_2360), and Program for Young Talents in China used to support the research of the manuscript.

### Notes

The authors declare no competing financial interest.

### ACKNOWLEDGMENTS

This work was supported by the National Key R&D Program of China (grant no. 2021YFC2100100), the General Program of National Natural Science Foundation of China (grant no. 22178146), and the Key R&D Program of Jiangsu Province (grant no. BE2020341-1), Postgraduate Research&Practice Innovation Program of Jiangsu Province (grant no. KVCX22\_2360), and Program for Young Talents in China supported the research in the manuscript. The author thanks Danyu GU from Instrumentation and Service Center for Molecular Sciences at Westlake University for the assistance in stopped flow spectrum measurement.

### ABBREVIATIONS

LAO, L-amino acid oxidase; RoLAO, L-amino acid oxidase from *Rhodococcus opacus*; TTN, total turnover number; S, substrate; Int, intermediate; TS, transition state; STY, space-time yields; AKR, aldo-keto reductase; QM/MM, quantum mechanics/molecular mechanics; RMSD, root-mean-square deviation; SBD, substrate-binding domain; FBD, FAD-binding domain; HD, helical domain; FAD<sub>M</sub>, a FAD-truncated model; CrLAO, L-amino acid oxidase from *Calloselasma rhodostoma*; H, hydride ion;  $\alpha$ -PPA,  $\alpha$ -phenylpyruvic acid;  $\alpha$ -KIV,  $\alpha$ -ketoisovalerate;  $\alpha$ -KMTB,  $\alpha$ -keto- $\gamma$ -methylthiobutyric acid;  $\alpha$ -KIC,  $\alpha$ -ketoisocaproate; UHPLC, ultrahigh performance liquid

chromatography; DFT, density functional theory; 3CL<sup>Pro</sup>, coronavirus 3C-like protease; Thal, tryptophan 6-halogenase;  $\omega$ -TA,  $\omega$ -transaminase; LAAD, L-amino acid deaminase

### REFERENCES

- (1) Calcio Gaudino, E.; Grillo, G.; Tabasso, S.; Stevanato, L.; Cravotto, G.; Marjamaa, K.; Pihlajaniemi, V.; Koivula, A.; Aro, N.; Uusitalo, J.; Ropponen, J.; Kuutti, L.; Kivinen, P.; Kanerva, H.; Arshanita, A.; Jashina, L.; Jurkjane, V.; Andersone, A.; Dreyer, T.; Schories, G. Optimization of ultrasound pretreatment and enzymatic hydrolysis of wheat straw: From lab to semi-industrial scale. *J. Clean Prod.* **2022**, *380*, 1–20.
- (2) Romero, E.; Gomez Castellanos, J. R.; Gadda, G.; Fraaije, M. W.; Mattevi, A. Same substrate, many reactions: Oxygen activation in flavoenzymes. *Chem. Rev.* **2018**, *118* (4), 1742–1769.
- (3) Yi, D.; Bayer, T.; Badenhorst, C. P. S.; Wu, S. K.; Doerr, M.; Hohne, M.; Bornscheuer, U. T. Recent trends in biocatalysis. *Chem. Soc. Rev.* **2021**, *50* (14), 8003–8049.
- (4) Simic, S.; Zukic, E.; Schmermund, L.; Faber, K.; Winkler, C. K.; Kroutil, W. Shortening synthetic routes to small molecule active pharmaceutical ingredients employing biocatalytic methods. *Chem. Rev.* **2022**, *122* (1), 1052–1126.
- (5) Mirmohamadsadeghi, S.; Karimi, K.; Azarbaijani, R.; Parsa Yeganeh, L.; Angelidaki, I.; Nizami, A. S.; Bhat, R.; Dashora, K.; Vijay, V. K.; Aghbashlo, M.; Gupta, V. K.; Tabatabaei, M. Pretreatment of lignocelluloses for enhanced biogas production: A review on influencing mechanisms and the importance of microbial diversity. *Renewable Sustainable Energy Rev.* **2021**, *135*, 1–18.
- (6) Bell, E. L.; Smithson, R.; Kilbride, S.; Foster, J.; Hardy, F. J.; Ramachandran, S.; Tedstone, A. A.; Haigh, S. J.; Garforth, A. A.; Day, P. J. R.; Levy, C.; Shaver, M. P.; Green, A. P. Directed evolution of an efficient and thermostable PET depolymerase. *Nat. Catal.* **2022**, *5* (8), 673–681.
- (7) Deng, L.; Wang, Z.; Jiang, X.; Xu, J.; Zhou, Z.; Li, X.; You, Z.; Ding, M.; Shishido, T.; Liu, X.; Xu, M. Catalytic aqueous CO<sub>2</sub> reduction to formaldehyde at Ru surface on hydroxyl-groups-rich LDH under mild conditions. *Appl. Catal., B* **2023**, *322*, 1–11.
- (8) Wei, R.; von Haugwitz, G.; Pfaff, L.; Mican, J.; Badenhorst, C. P. S.; Liu, W. D.; Weber, G.; Austin, H. P.; Bednar, D.; Damborsky, J.; Bornscheuer, U. T. Mechanism-based design of efficient PET hydrolases. *ACS Catal.* **2022**, *12* (6), 3382–3396.
- (9) Tian, C.; Yang, J.; Liu, C.; Chen, P.; Zhang, T.; Men, Y.; Ma, H.; Sun, Y.; Ma, Y. Engineering substrate specificity of HAD phosphatases and multienzyme systems development for the thermodynamic-driven manufacturing sugars. *Nat. Commun.* **2022**, *13* (1), 1–13.
- (10) Pultz, I. S.; Hill, M.; Vitanza, J. M.; Wolf, C.; Saaby, L.; Liu, T. N.; Winkle, P.; Leffler, D. A. Gluten degradation, pharmacokinetics, safety, and tolerability of TAK-062, an engineered enzyme to treat celiac disease. *Gastroenterology* **2021**, *161* (1), 81–93.
- (11) Wu, L.; Qin, L.; Nie, Y.; Xu, Y.; Zhao, Y. L. Computer-aided understanding and engineering of enzymatic selectivity. *Biotechnol. Adv.* **2022**, *54*, 1–20.
- (12) Li, M.; Blum, N. T.; Wu, J.; Lin, J.; Huang, P. Weaving enzymes with polymeric shells for biomedical applications. *Adv. Mater.* **2021**, *33* (34), 1–18.
- (13) Qian, Y. Y.; Lu, C.; Liu, J.; Song, W.; Chen, X. L.; Luo, Q. L.; Liu, L. M.; Wu, J. Engineering protonation conformation of L-aspartate- $\alpha$ -decarboxylase to relieve mechanism-based inactivation. *Biotechnol. Bioeng.* **2020**, *117* (6), 1607–1614.
- (14) Wang, L.; Song, W.; Wang, B. J.; Zhang, Y.; Xu, X.; Wu, J.; Gao, C.; Liu, J.; Chen, X. L.; Chen, J. H.; Liu, L. M. One-pot enzymatic-chemical cascade route for synthesizing aromatic  $\alpha$ -hydroxy ketones. *ACS Catal.* **2021**, *11* (5), 2808–2818.
- (15) Gao, D.; Song, W.; Wu, J.; Guo, L.; Gao, C.; Liu, J.; Chen, X.; Liu, L. Efficient production of L-homophenylalanine by enzymatic-chemical cascade catalysis. *Angew. Chem., Int. Ed.* **2022**, *61* (36), No. e202207077.

- (16) Wei, W.; Ettelaie, R.; Zhang, X.; Fan, M.; Dong, Y.; Li, Z.; Yang, H. Co-compartmentalization of enzymes and cofactors within pickering emulsion droplets for continuous-flow catalysis. *Angew. Chem., Int. Ed.* **2022**, *61* (45), No. e202211912.
- (17) Deng, H.; Ma, Y.; Ren, W.-S.; Vuong, V. Q.; Qian, P.; Guo, H. Structure and dynamics of the reactive state for the histidine methylation process and catalytic mechanism of SETD3: Insights from quantum mechanics/molecular mechanics investigation. *ACS Catal.* **2020**, *10* (22), 13314–13322.
- (18) Nochebuena, J.; Naseem-Khan, S.; Cisneros, G. A. Development and application of quantum mechanics/molecular mechanics methods with advanced polarizable potentials. *Wiley Interdiscip. Rev. Comput. Mol. Sci.* **2021**, *11* (4), 27.
- (19) Lin, H. Y.; Chen, X.; Dong, J.; Yang, J. F.; Xiao, H.; Ye, Y.; Li, L. H.; Zhan, C. G.; Yang, W. C.; Yang, G. F. Rational Redesign of enzyme via the combination of quantum mechanics/molecular mechanics, molecular dynamics, and structural biology study. *J. Am. Chem. Soc.* **2021**, *143* (38), 15674–15687.
- (20) Shi, J.; Shi, Y.; Li, J. C.; Wei, W.; Chen, Y.; Cheng, P.; Liu, C. L.; Zhang, H.; Wu, R.; Zhang, B.; Jiao, R. H.; Yu, S.; Liang, Y.; Tan, R. X.; Ge, H. M. In vitro reconstitution of cinnamoyl moiety reveals two distinct cyclases for benzene ring formation. *J. Am. Chem. Soc.* **2022**, *144* (17), 7939–7948.
- (21) Lonhienne, T.; Low, Y. S.; Garcia, M. D.; Croll, T.; Gao, Y.; Wang, Q.; Brillault, L.; Williams, C. M.; Fraser, J. A.; McGeary, R. P.; West, N. P.; Landsberg, M. J.; Rao, Z.; Schenk, G.; Guddat, L. W. Structures of fungal and plant acetohydroxyacid synthases. *Nature* **2020**, *586* (7828), 317–321.
- (22) Jang, C.; Chen, L.; Rabinowitz, J. D. Metabolomics and isotope tracing. *Cell* **2018**, *173* (4), 822–837.
- (23) Song, W.; Xu, X.; Gao, C.; Zhang, Y. X.; Wu, J.; Liu, J.; Chen, X. L.; Luo, Q. L.; Liu, L. M. Open gate of *Corynebacterium glutamicum* Threonine deaminase for efficient synthesis of bulky alpha-keto acids. *ACS Catal.* **2020**, *10* (17), 9994–10004.
- (24) Goel, M.; Siegert, M.; Krauss, G.; Mohanraj, J.; Hochgesang, A.; Heinrich, D. C.; Fried, M.; Pflaum, J.; Thelakkat, M. HOMO-HOMO electron transfer: An elegant strategy for p-type doping of polymer semiconductors toward thermoelectric applications. *Adv. Mater.* **2020**, *32* (43), 1–7.
- (25) Li, W.; He, D.; Sheehan, S. W.; He, Y. M.; Thorne, J. E.; Yao, X. H.; Brudvig, G. W.; Wang, D. W. Comparison of heterogenized molecular and heterogeneous oxide catalysts for photoelectrochemical water oxidation. *Energy Environ. Sci.* **2016**, *9* (5), 1794–1802.
- (26) Pukala, T.; Robinson, C. V. Introduction: Mass spectrometry applications in structural biology. *Chem. Rev.* **2022**, *122* (8), 7267–7268.
- (27) Centurion, M. Structural dynamics in molecules observed with femtosecond X-ray pulses. *Chem.* **2019**, *5* (9), 2293–2295.
- (28) Fu, Y.; Bernasconi, L.; Liu, P. Ab initio molecular dynamics simulations of the  $S_N1/S_N2$  mechanistic continuum in glycosylation Reactions. *J. Am. Chem. Soc.* **2021**, *143* (3), 1577–1589.
- (29) Araki, M.; Matsumoto, S.; Bekker, G. J.; Isaka, Y.; Sagae, Y.; Kamiya, N.; Okuno, Y. Exploring ligand binding pathways on proteins using hypersound-accelerated molecular dynamics. *Nat. Commun.* **2021**, *12* (1), 2793.
- (30) Yang, L.; Zhang, K.; Xu, M.; Xie, Y.; Meng, X.; Wang, H.; Wei, D. Mechanism-guided computational design of omega-Transaminase by reprogramming of high-energy-barrier steps. *Angew. Chem.-Int. Ed.* **2022**, *61* (52), No. e202212555.
- (31) Sanz-Martinez, I.; García-García, A.; Tejero, T.; Hurtado-Guerrero, R.; Merino, P. The essential role of water molecules in the reaction mechanism of protein O-fucosyltransferase 2. *Angew. Chem., Int. Ed.* **2022**, *61* (48), No. e202213610.
- (32) Rindfleisch, S.; Krull, M.; Uranga, J.; Schmidt, T.; Rabe von Pappenheim, F.; Kirck, L. L.; Balouri, A.; Schneider, T.; Chari, A.; Kluger, R.; Bourenkov, G.; Diederichsen, U.; Mata, R. A.; Tittmann, K. Ground-state destabilization by electrostatic repulsion is not a driving force in orotidine-5'-monophosphate decarboxylase catalysis. *Nat. Catal.* **2022**, *5* (4), 332–341.
- (33) Lai, R.; Cui, Q. How to stabilize carbenes in enzyme active sites without metal ions. *J. Am. Chem. Soc.* **2022**, *144* (45), 20739–20751.
- (34) Waheed, S. O.; Chaturvedi, S. S.; Karabencheva-Christova, T. G.; Christov, C. Z. Catalytic mechanism of human ten-eleven translocation-2 (TET2) enzyme: Effects of conformational changes, electric field, and mutations. *ACS Catal.* **2021**, *11* (7), 3877–3890.
- (35) Cichos, F.; Gustavsson, K.; Mehlig, B.; Volpe, G. Machine learning for active matter. *Nat. Mach. Intell.* **2020**, *2* (2), 94–103.
- (36) Liu, N.; Wu, L.; Feng, J.; Sheng, X.; Li, J.; Chen, X.; Li, J.; Liu, W.; Zhou, J.; Wu, Q.; Zhu, D. Crystal structures and catalytic mechanism of l-erythro-3,5-diaminohexanoate dehydrogenase and rational engineering for asymmetric synthesis of beta-amino acids. *Angew. Chem.-Int. Ed.* **2021**, *60* (18), 10203–10210.
- (37) Garcia-Borras, M.; Kan, S. B. J.; Lewis, R. D.; Tang, A.; Jimenez-Osca, G.; Arnold, F. H.; Houk, K. N. Origin and control of chemoselectivity in Cytochrome c catalyzed carbene transfer into Si-H and N-H bonds. *J. Am. Chem. Soc.* **2021**, *143* (18), 7114–7123.
- (38) Song, Y.; Li, J.; Shin, H.-D.; Liu, L.; Du, G.; Chen, J. Biotechnological production of alpha-keto acids: Current status and perspectives. *Bioresour. Technol.* **2016**, *219*, 716–724.
- (39) Luo, Z.; Yu, S.; Zeng, W.; Zhou, J. Comparative analysis of the chemical and biochemical synthesis of keto acids. *Biotechnol. Adv.* **2021**, *2021* (47), No. 107706.
- (40) Hu, X.; Wang, J.; Yang, H.; Ji, S.; Li, Y.; Xu, B.; Cui, H. Bailing Capsule combined with  $\alpha$ -ketoacid tablets for stage 3 chronic kidney disease: Protocol of a double-blinded, randomized, controlled trial. *Medicine* **2021**, *100* (20), No. e25759.
- (41) Wang, M.; Xu, H.; Chong Lee Shin, O. L. S.; Li, L.; Gao, H.; Zhao, Z.; Zhu, F.; Zhu, H.; Liang, W.; Qian, K.; Zhang, C.; Zeng, R.; Zhou, H.; Yao, Y. Compound  $\alpha$ -keto acid tablet supplementation alleviates chronic kidney disease progression via inhibition of the NF- $\kappa$ B and MAPK pathways. *J. Transl. Med.* **2019**, *17* (122), 1–15.
- (42) Faust, A.; Niefind, K.; Hummel, W.; Schomburg, D. The structure of a bacterial L-amino acid oxidase from *Rhodococcus opacus* gives new evidence for the hydride mechanism for dehydrogenation. *J. Mol. Biol.* **2007**, *367* (1), 234–48.
- (43) Geueke, B.; Hummel, W. A new bacterial l-amino acid oxidase with a broad substrate specificity: purification and characterization. *Enzyme Microb. Technol.* **2002**, *31*, 77–87.
- (44) Qi, N.; Liu, J. M.; Song, W.; Liu, J.; Gao, C.; Chen, X. L.; Guo, L.; Liu, L. M.; Wu, J. Rational design of Phospholipase D to improve the transphosphatidylase activity for phosphatidylserine synthesis. *J. Agric. Food Chem.* **2022**, *70* (22), 6709–6718.
- (45) Cramer, P. AlphaFold2 and the future of structural biology. *Nat. Struct. Mol. Biol.* **2021**, *28* (9), 704–705.
- (46) Kiss, D. J.; Ferenczy, G. G. A detailed mechanism of the oxidative half-reaction of D-amino acid oxidase: another route for flavin oxidation. *Org. Biomol. Chem.* **2019**, *17* (34), 7973–7984.
- (47) Wu, Y. Y.; Zhang, S.; Song, W.; Liu, J.; Chen, X. L.; Hu, G. P.; Zhou, Y. W.; Liu, L. M.; Wu, J. Enhanced catalytic efficiency of L-amino acid deaminase achieved by a shorter hydride transfer distance. *ChemCatChem.* **2021**, *13* (21), 4557–4566.
- (48) Moustafa, I. M.; Foster, S.; Lyubimov, A. Y.; Vrieling, A. Crystal structure of LAAO from *Calloselasma rhodostoma* with an L-phenylalanyl substrate: Insights into structure and mechanism. *J. Mol. Biol.* **2006**, *364* (5), 991–1002.
- (49) Sikora, L.; Marzluf, G. A. Regulation of L-amino-acid oxidase and of D-amino-acid oxidase in *Neurospora crassa*. *Mol. Gen. Genet.* **1982**, *186* (186), 33–39.
- (50) Wang, H.; He, S.; Deng, W.; Zhang, Y.; Li, G.; Sun, J.; Zhao, W.; Guo, Y.; Yin, Z.; Li, D.; Shang, L. Comprehensive insights into the catalytic mechanism of middle east respiratory syndrome 3C-Like Protease and severe acute respiratory syndrome 3C-Like Protease. *ACS Catal.* **2020**, *10*, 5871–5890.
- (51) Prakinee, K.; Phintha, A.; Visitsathawong, S.; Lawan, N.; Sucharitakul, J.; Kantiwiriyawanitch, C.; Damborsky, J.; Chitnumsub, P.; van Pée, K.-H.; Chaiyen, P. Mechanism-guided tunnel engineering to increase the efficiency of a flavin-dependent halogenase. *Nat. Catal.* **2022**, *5* (6), 534–544.

- (52) Marshall, J. R.; Yao, P.; Montgomery, S. L.; Finnigan, J. D.; Thorpe, T. W.; Palmer, R. B.; Mangas-Sanchez, J.; Duncan, R. A. M.; Heath, R. S.; Graham, K. M.; Cook, D. J.; Charnock, S. J.; Turner, N. J. Screening and characterization of a diverse panel of metagenomic imine reductases for biocatalytic reductive amination. *Nat. Chem.* **2021**, *13* (2), 140–148.
- (53) Fan, X. C.; Chen, R. D.; Chen, L. L.; Liu, L. M. Enhancement of alpha-ketoglutaric acid production from *L*-glutamic acid by high-cell-density cultivation. *J. Mol. Catal. B-Enzym.* **2016**, *126*, 10–17.
- (54) Busch, F.; Brummund, J.; Calderini, E.; Schurmann, M.; Kourist, R. Cofactor generation cascade for alpha-Ketoglutarate and Fe(II)-Dependent Dioxygenases. *ACS Sustainable Chem. Eng.* **2020**, *8* (23), 8604–8612.
- (55) Yuan, Y. X.; Song, W.; Liu, J.; Chen, X. L.; Luo, Q. L.; Liu, L. M. Production of alpha-ketoisocaproate and alpha-keto-beta-methylvalerate by engineered *L*-amino acid deaminase. *ChemCatChem.* **2019**, *11* (10), 2464–2472.
- (56) Schmitz, M.; Schultze, A.; Vanags, R.; Voigt, K.; Di Ventura, B.; Öztürk, M. A. patchwork: a user-friendly pH sensitivity analysis web server for protein sequences and structures. *Nucleic Acids Res.* **2022**, *50*, 560–567.
- (57) Seminario, J. M. Calculation of intramolecular force fields from second-derivative tensors. *Int. J. Quantum Chem.* **1996**, *60* (7), 1271–1277.
- (58) Takano, Y.; Houk, K. N. Benchmarking the conductor-like polarizable continuum model (CPCM) for aqueous solvation free energies of neutral and ionic organic molecules. *J. Chem. Theory Comput.* **2005**, *1* (1), 70–77.
- (59) Tang, S.; Chen, R.; Lin, M.; Lin, Q.; Zhu, Y.; Ding, J.; Hu, H.; Ling, M.; Wu, J. Accelerating AutoDock Vina with GPUs. *Molecules* **2022**, *27* (9), 1–18.
- (60) Case, D. A.; Walker, R. C.; III, T. E. C.; Simmerling, C.; Roitberg, A.; Merz, K. M.; Li, P.; Luo, R.; Darden, T.; Sagui, C.; Pan, F.; Wang, J.; Roe, D. R. *Amber 18*. University of California: San Francisco, 2018.
- (61) Jakalian, A.; Jack, D. B.; Bayly, C. I. Fast, efficient generation of high-quality atomic charges. AM1-BCC model: II. Parameterization and validation. *J. Comput. Chem.* **2002**, *23* (16), 1623–1641.
- (62) He, X.; Man, V. H.; Yang, W.; Lee, T. S.; Wang, J. A fast and high-quality charge model for the next generation general AMBER force field. *J. Chem. Phys.* **2020**, *153* (11), 1–11.
- (63) Symons, B. C. B.; Popelier, P. L. A. Flexible multipole moments in smooth particle mesh Ewald. *J. Chem. Phys.* **2022**, *156* (24), 1–10.
- (64) Frisch, M. J.; Trucks, G. W.; Schlegel, H. B.; Scuseria, G. E.; Robb, M. A.; Cheeseman, J. R.; Scalmani, G.; Barone, V.; Petersson, G. A.; Nakatsuji, H.; Li, X.; Caricato, M.; Marenich, A. V.; Bloino, J.; Janesko, B. G.; Gomperts, R.; Mennucci, B.; Hratchian, H. P.; Ortiz, J. V.; Izmaylov, A. F.; Sonnenberg, J. L.; Williams, D.; Ding, F.; Lipparini, F.; Egidi, F.; Goings, J.; Peng, B.; Petrone, A.; Henderson, T.; Ranasinghe, D.; Zakrzewski, V. G.; Gao, J.; Rega, N.; Zheng, G.; Liang, W.; Hada, M.; Ehara, M.; Toyota, K.; Fukuda, R.; Hasegawa, J.; Ishida, M.; Nakajima, T.; Honda, Y.; Kitao, O.; Nakai, H.; Vreven, T.; Throssell, K.; Montgomery, Jr., J. A.; Peralta, J. E.; Ogliaro, F.; Bearpark, M. J.; Heyd, J. J.; Brothers, E. N.; Kudin, K. N.; Staroverov, V. N.; Keith, T. A.; Kobayashi, R.; Normand, J.; Raghavachari, K.; Rendell, A. P.; Burant, J. C.; Iyengar, S. S.; Tomasi, J.; Cossi, M.; Millam, J. M.; Klene, M.; Adamo, C.; Cammi, R.; Ochterski, J. W.; Martin, R. L.; Morokuma, K.; Farkas, O.; Foresman, J. B.; Fox, D. J. *Gaussian 16 Rev. C.01*; Gaussian Inc.: Wallingford, CT, 2016.
- (65) Liu, Z.; Rivera, S.; Newmister, S. A.; Sanders, J. N.; Nie, Q.; Liu, S.; Zhao, F.; Ferrara, J. D.; Shih, H.-W.; Patil, S.; Xu, W.; Miller, M. D.; Phillips, G. N.; Houk, K. N.; Sherman, D. H.; Gao, X. An NmrA-like enzyme-catalysed redox-mediated Diels–Alder cycloaddition with anti-selectivity. *Nat. Chem.* **2023**, *15*, 526–534.
- (66) Miertuš, S.; Scrocco, E.; Tomasi, J. Electrostatic interaction of a solute with a continuum. A direct utilization of AB initio molecular potentials for the prevision of solvent effects. *Chem. Phys.* **1981**, *55*, 117–129.
- (67) Miertuš, S.; Tomasi, J. Approximate evaluations of the electrostatic free energy and internal energy changes in solution processes. *Chem. Phys.* **1982**, *65*, 239–245.
- (68) Pascual-ahuir, J. L.; Silla, E.; Tuñon, I. GEPOL: An improved description of molecular surfaces. III. A new algorithm for the computation of a solvent-excluding surface. *J. Comput. Chem.* **1994**, *15*, 1127–1138.